High-Performance Mild Annealed CNT/GO-PVA Composite Membrane for Brackish Water Treatment

Sudesh Yadav[1], Ibrar Ibrar[1], Ali Altaee[1, #], Akshaya K. Samal[2], Elika Karbassiyazdi[1], John Zhou[1], Pietro Bartocci[3]

1: Centre for Green Technology, School of Civil and Environmental Engineering, University of Technology Sydney, 15 Broadway, NSW, 2007, Australia

2: Centre for Nano and Material Sciences, Jain University, Jain Global Campus, Ramanagara, Bangalore - 562112, India

3: Department of Engineering, University of Perugia, Via G. Duranti 67, Perugia 06125, Italy

4: 2Instituto de Carboquímica (ICB-CSIC), Miguel Luesma Castán 4, 50018, Zaragoza, Spain

email: pbartocci@icb.csic.es

Corresponding author email address: ali.altaee@uts.edu.au

Abstract

Two-dimensional (2D) graphene oxide (GO)-based materials with tunable physicochemical properties have enormous potential for developing next-generation desalination membranes. Nevertheless, weak interlamellar interactions result in poor selectivity towards small ions, limiting the wide applicability of GO membranes. Controlling the swelling of the GO membrane while maintaining high permeability and selectivity is a significant scientific and technological challenge. To address the issues above, we used one-dimensional (ID) carbon nanotubes (CNT) as a nano-spacer and polyvinyl alcohol (PVA) as an adhesive. Synergistic ionic complexation between 1D-CNT, 2D-GO, and PVA was studied using various analytical techniques. The intercalation of CNT between GO nanosheets and the cross-linking of CNT/GO-PVA significantly improved the separation performance. Pressure-assisted filtration was used to coat the CNT/GO-PVA on hydrophilic mixed cellulose esters (MCE) support with pore size 0.22 µm to obtain a highly ordered laminated structure. Five minutes of mild annealing at 80 °C narrowed the laminar channels of the GO nanosheets by transforming the oxygen-containing functional groups. In a dead-end filtration unit, the

CNT_5/GO_{15}-$PVA_{0.5}$ composite membrane exhibits a high rejection of 94.2% to sodium sulphate (Na_2SO_4) and 85.86% to sodium chloride (NaCl), accompanied by a high permeate rate of 14.2-13.45 LMH at 5 bar operating pressure. The salt rejection studies were evaluated for continuous operation for 72 hours for all membranes. Due to the synergistic effect of CNT, GO, and PVA, prepared membranes demonstrated the potential for practical water separation applications with desired permeability and selectivity.

Keywords: graphene oxide, carbon nanotube, swelling, membrane separation, desalination

1. Introduction

Nanofiltration (NF) technology applications for hard water softening, resource recovery and desalination processes are numerous [1, 2]. Polymeric NF membranes were widely used for ions separation at relatively low pressure and demonstrated high efficiency in removing divalent ions and, to a less extent, monovalent ions [2, 3]. Despite the several advantages of NF membranes, polymeric NF membranes experience some drawbacks, such as limited water flux, membrane fouling, and low rejection of monovalent ions [4, 5]. Researchers suggested incorporating nanomaterials in polymeric NF membranes to improve their filtration characteristics and fouling propensity [6].

Graphene-based materials are state-of-the-art with potential applications in batteries, composite materials, and separation and purification technologies due to their excellent physicochemical properties [7-9]. The intertwined nanochannels formed by the stacking of 2D graphene-based nanosheets in graphene-based membranes result in a zigzag route for the permeation of water molecules [10]. Graphene oxide (GO) membranes are gaining wide attention in the preparation of NF membranes due to the ease of fabrication via various methods, e.g. pressure-assisted filtration [11], inkjet printing [12], vacuum, and dip-coating method [13]. Among all the methods mentioned above, pressure-assisted filtration is widely applied to obtain GO membranes' highly ordered laminar structure [11, 14]. One of the GO-based membrane limitations is that polar functional groups of the GO sheets increase the interlayer spacing to about 7 nm when exposed to an aqueous environment [15]. Previous studies showed that the reduction in membrane thickness (< 100 nm) effectively increases the permeability of the GO membrane but compromises its selectivity [11, 16, 17]. The selectivity of the GO-based membranes is governed by the surface charge and the frictionless

capillary channels for mass transport [18]. The post-treatment process and fabrication technique determine the formation of capillary channels and the microstructure order in GO membranes [18, 19]. Numerous strategies were developed to combat the swelling and instability of the GO membrane, such as chemical modification, reduction, and cross-linking of GO, enhancing the practical implementation of GO membranes in water and wastewater treatment [17]. Nevertheless, the partial reduction of polar functional groups of GO membranes could offer a stable NF membrane of a high rejection rate [20, 21].

Reduced graphene oxide (rGO) membranes are still under development and require more research to improve the permeability and rejection rate of the membrane. [22]. The rGO membranes resemble the properties of graphene materials with a lattice parameter of 3.5Å, which can potentially block salt ions by size exclusion [21]. Remarkably, tuning the interlayer spacing of graphene sheets using nanoparticles becomes an effective method for increasing the membrane's permeability. Laminated rGO membranes were obtained in previous studies by post-treatment of the GO membranes at a thermal temperature above 120 °C, but a decrease in membrane selectivity was reported due to the development of microstructural defects [23, 24]. Thus, a mild reduction of GO membranes is suggested to lower the transformation of polar functional groups with microstructure evolution at 80 °C. It is also postulated that the narrow interlayer space of graphene-based membranes is the main reason for its low water flux. Researchers investigated inorganic [25, 26], organic [19, 27, 28], and nanotubes-based frameworks [29, 30] nanoparticles for tuning the interlayer spacing in the GO membranes. Carbon nanotube (CNT) is considered the most promising material among all materials mentioned above due to its high compatibility [31]. For instance, Gao et al. [29] developed a graphene-based NF membrane intercalated with a multiwalled carbon nanotube (MWCNT) to improve salt rejection. The permeability coefficient of the developed membranes was 11.3 $Lm^{-2}h^{-1}bar^{-1}$ with a rejection rate of sodium sulfate (Na_2SO_4) and sodium chloride (NaCl) equal to 83.5% and 51.4%, respectively [29]. Another study by Jin et al. [30] prepared GO membranes intercalated with single-walled carbon nanotube (SWCNT). They have achieved water permeability up to 660–720 $Lm^{-2}h^{-1}bar^{-1}$ and a rejection rate of 97.4% to 98.7% to rhodamine B and coomassie brilliant blue dyes, respectively [30]. Fan et al. prepared loose NF membranes using rGO/CNT using block copolymers (BCPs) to disperse CNT for the removal of organic dyes and achieved 97.3% rejection for methyl orange (MO) dye

[32]. In another study, Huang et al. prepared rGO/CNT composite membranes for pharmaceuticals and personal care products (PPCP) [33]. They have achieved over 76% removal efficiency for PPCP with clean water permeability (4454 LMH/Bar) [33]. The rejection rate of rGO/CNT membrane to monovalent and divalent ions was not investigated in the previous studies. Future research should focus on improving the selectivity and stability of graphene-based membranes for desalination processes with enhanced antifouling performance.

In this study, mild annealed reduced graphene oxide (MrGO) membranes were prepared for water desalination at 80 °C. The fabricated membrane was cross-linked with optimal polyvinyl alcohol (PVA) concentration to stabilise the process and prevent membrane swelling. CNT was used to provide frictionless capillary channels for enhanced water permeability. The concentration of CNT in the graphene-based membranes was optimised for the trade-off between permeability and selectivity. Deionized (DI) water was used to prepare the GO/CNT-PVA dispersions for membrane fabrication. The GO/CNT-PVA membranes were tested for 2000 ppm sodium sulfate (Na_2SO_4) and sodium chloride (NaCl) rejection at 5 bar hydraulic pressure.

2. Materials and methods

2.1. Chemicals required

All chemicals used in this study were of analytical grade and used as received without any further purification. Brownish-yellow powder of high surface area GO of ≥ 99% purity with lateral size of 1-5 µm, and thickness of 0.8-1.2 nm was purchased from ACS Material, LLC, USA. The obtained GO has 51.26 and 40.78 wt. % of carbon and oxygen content, respectively. Multiwalled carbon nanotube (MWCNT) of ≥ 99% purity (Average diameter: 8.7-10 nm, Surface area: 216 m^2/g, and Trace metals analysis ≤ 20000 ppm). Polyvinyl alcohol (PVA) with an average molecular weight of 47 kDa, Na_2SO_4 and, NaCl chemicals were obtained from Merck, Australia. Hydrophilic mixed cellulose esters (MCE) MF-Millipore membrane filter (Pore size: 0.22 µm, Diameter: 47 mm, and Lot: R9NA98005) was supplied by Sigma Aldrich Australia.

2.2. MrGO/CNT-PVA membrane fabrication

In the beginning, 5 g of PVA was dissolved in 100 mL DI water for 24 hours at 60 °C with constant stirring. The resulting viscous solution was sonicated for an hour to remove any trapped air bubbles. Next, aqueous GO and CNT (25 mg/l) were prepared using an ultrasonication bath for 2 hours with 60 °C temperature at 40 kHz. Terminology and the composition of all the prepared solutions for coating are in **Table 1**. The GO/CNT-PVA composite membranes were prepared using a pressure-assisted filtration technique, as depicted in **Figure 1**. The solutions were passed through hydrophilic mixed cellulose esters (MCE) filters with 0.22 μm pore size at 5 bar pressure for 3 hours. The obtained membranes were dried overnight at room temperature (23 ± 1.5 °C) and thermally reduced at 80 °C for 5 min to obtain MrGO. Finally, the obtained membranes were characterised using various analytical instruments listed in **Table 2**. Before conducting the performance studies, the obtained GO/CNT-PVA composite membranes were stored in plastic Petri dishes.

Table 1: Composition of GO, CNT and PVA in the various coating solutions to prepare GO/CNT-PVA composite membranes.

Membrane code	**CNT**		**GO**		**PVA (5 wt% (mL))**	
	Aq sol, mL	**Volume ratio (%)**	**Aq sol, mL**	**Volume ratio (%)**	**5 wt% (mL)**	**Volume ratio (%)**
$CNT_5GO_{15}PVA_{0.5}$	5	24.39	15	73.17	0.5	2.44
$CNT_{10}GO_{10}PVA_{0.5}$	10	48.78	10	48.78	0.5	2.44
$CNT_{15}GO_5PVA_{0.5}$	15	73.17	5	24.39	0.5	2.44
$GO_{20}PVA_{0.5}$	-	-	20	97.56	0.5	2.44
$CNT_{20}PVA_{0.5}$	20	97.56	-	-	0.5	2.44
CNT_{20}	20	100	-	-	-	-

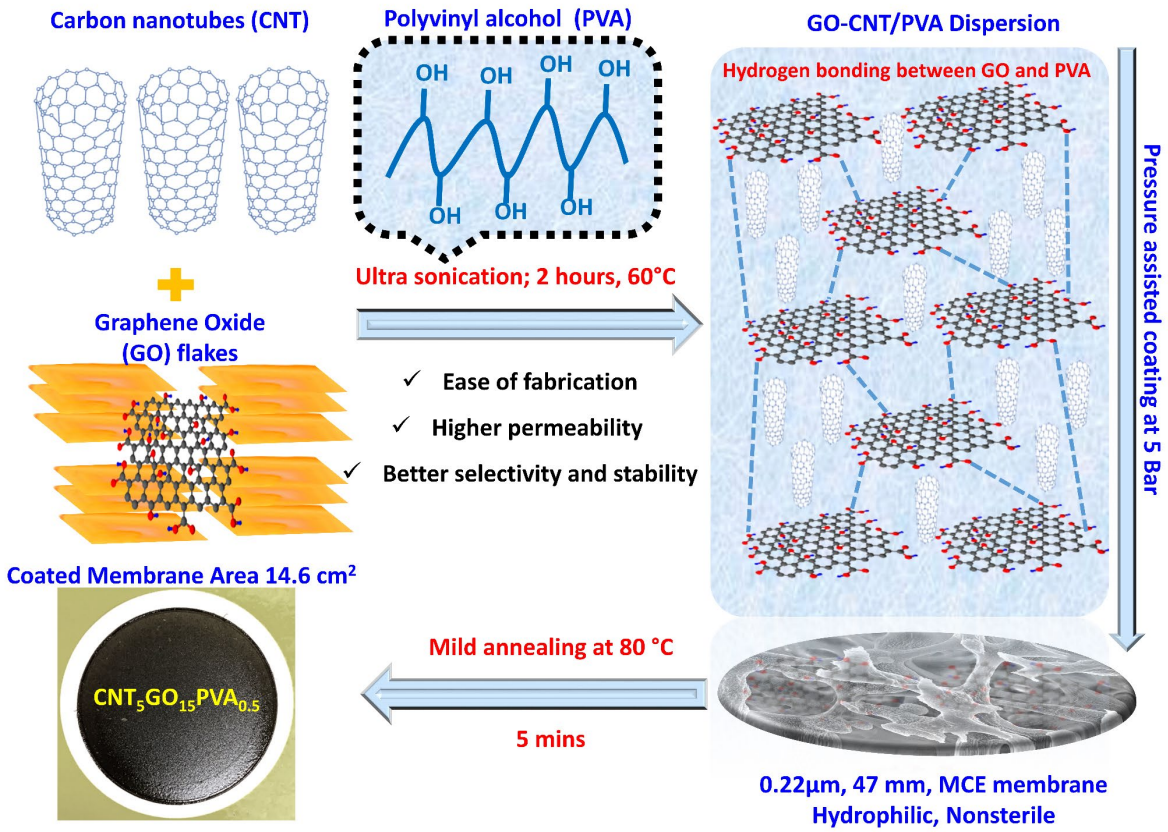

Figure 1: Schematic illustration for the fabrication of GO/CNT-PVA composite membranes.

Table 2: Analytical instruments used to study the physicochemical properties of GO/CNT-PVA composite membranes.

Analytical instrument	Physiochemical properties studied
Fourier-transform infrared spectroscopy (FTIR)	To identify the functional groups and chemical bonds
Raman spectroscopy	To study the phonon properties of CNT and GO and to detect vibrational and rotational states in a molecular system
Scanning electron microscopy (SEM)	To investigate the morphology of the resultant membranes
X-ray diffraction (XRD)	To analyse the effective channel size (interlayer space) of the membranes
X-ray photoelectron spectroscopy (XPS)	To identify the chemical bonding and structure of the resultant membranes

Water contact angle studies	To study the hydrophilicity of the resultant membrane
Surface zeta (ζ) potential measurements	To measure the magnitude of the electrostatic or charge repulsion/attraction at the interface

2.3. Membrane performance studies

Membrane performance studies (pure water flux and salt rejection) were conducted using HP4750 Sterlitech cell at 23 ± 1.5 °C temperature and ~ 48 ± 4 % humidity. The HP4750 Sterlitech cell had an active membrane area (A) of 0.00146 m^2, and the cell was filled with feed every 12 hours. The first 30 minutes of operation were used to stabilise the system prior to taking the readings. All experiments were carried out at a constant hydraulic pressure of 5 bar supplied by compressed air. Using an electronic weighing balance, permeate flux was calculated every three hours for the first 12 hours of operation and then every 12, 24, and 24 hours. The permeate flux (*J*) and salt rejection rate were calculated using equations 1 and 2, respectively. In the Equations, V denotes the volume of permeate in litres (L), and t denotes the time in hours. C_p and C_f represent the salt concentrations in permeate and feed, respectively, as determined by the LAQUA PC210 conductivity metre. Each experiment was carried out three times, with the average value reported.

$$J = \frac{V}{A \times t} \quad (1)$$

$$Rejection\,(\%) = \left(1 - \frac{C_p}{C_f}\right) \times 100 \quad (2)$$

3. Results and discussions

3.1. Physicochemical properties of the GO/CNT-PVA composite membranes

A significant challenge in designing and fabricating GO-based membranes is to ensure that molecular transport occurs entirely within the nanochannels and would not occur via membrane cracks or pores [34]. **Figure S1** shows the surface morphology of the MCE substrate. The top-surface morphologies of the GO/CNT-PVA composite membranes are shown in **Figure 2a**. Since CNT lack polar functional groups, agglomeration of CNT can be observed in the CNT_{20} and $CNT_{20}PVA_{0.5}$ membranes. Both membranes exhibited microscale

defects, indicating a lack of selectivity. Due to the non-uniform coating on CNT_{20} and $CNT_{20}PVA_{0.5}$ membranes, they were excluded from the performance studies. The surface morphology of the $CNT_5GO_{15}PVA_{0.5}$ membrane is nearly identical to that of the $GO_{20}PVA_{0.5}$ membrane, but the $GO_{20}PVA_{0.5}$ membrane exhibits a few more wrinkles. On the other hand, $CNT_{10}GO_{10}PVA_{0.5}$ and $CNT_{15}GO_5PVA_{0.5}$ membranes exhibited a mixture of morphologies, including i) a few agglomerated CNT on the top surface and ii) wrinkles caused by the GO and PVA. The wrinkles on $CNT_5GO_{15}PVA_{0.5}$ and $GO_{20}PVA_{0.5}$ might be due to the trapped air or water molecules between GO nanosheets during membrane fabrication. The cross-section of all the prepared membranes is shown in **Figure S3**. It is worth noting that the membrane thickness significantly impacts the selectivity and permeability characteristics, as a thinner coating layer promotes high water flux. Although increasing the GO content increased the thickness of membranes $CNT_5GO_{15}PVA_{0.5}$ and $GO_{20}PVA_{0.5}$, these membranes still showed slightly higher water permeability compared to membranes $CNT_{10}GO_{10}PVA_{0.5}$ and $CNT_{15}GO_5PVA_{0.5}$ membranes. The increased water permeability could be due to the positive effect of increasing the hydrophilicity and improved membrane surface properties that transcended the negative impact of the increased hydraulic resistance caused by a thicker membrane. This discrepancy can be attributed to the different ratios of the CNT and GO nanosheets used, which alter the interaction between water and nanosheets during the drying process, thereby altering how these nanosheets stack in dried membranes.

The CNT/GO-PVA composite membranes were prepared using aqueous suspensions of CNT/GO-PVA (**Figure S2**). Due to the presence of polar functional groups, a completely dispersed yellowish-brownish solution was obtained for $GO_{20}PVA_{0.5}$. The UV-visible spectrometer was used to determine the transparency of all coating solutions (**Figure 2b**). The $GO_{20}PVA_{0.5}$ solution exhibited greater than 84% transparency in the 380-750 nm wavelength range. Pristine CNT are hydrophobic and tend to agglomerate in DI water; therefore, almost a straight line was seen for the CNT_{20} solution. However, when GO and PVA were added, the solution became darker, and thus partial transparency for CNT/GO-PVA aqueous solutions was observed. This could be due to the Van der Waals interactions between CNT and PVA, as shown in **Figure 3a** [35]. Additionally, prolonged ultra-sonication of CNT solution reduces the aspect ratio of CNT, resulting in partial fragmentation of CNT. Thus, Van der Waals interactions between CNT and PVA, hydrogen bonding between GO and PVA,

and donor-acceptor π interactions between GO and CNT contribute to the stability of the aqueous solution $CNT_{15}GO_5PVA_{0.5}$, $CNT_{10}GO_{10}PVA_{0.5}$, $CNT_5GO_{15}PVA_{0.5}$ and, $GO_{20}PVA_{0.5}$. The typical GO membrane exhibits an intense (001) peak near 10.5 ° and an interlayer spacing of 8.4 Å [36]. The peak for CNT/GO-PVA composite membranes shift to 19.3 ° after prolonged ultra-sonication and mild annealing during the membrane fabrication process (**Figure 2c**). Apart from this, all (002) peaks in CNT/GO-PVA composite membranes are weak and have broad curves compared to the pristine GO membrane. This observation indicates a degraded crystalline structure following mild annealing, resulting from a partial reduction of polar functional groups. Hence, these XRD results confirm the structural changes caused by mild annealing, which further aids in enhanced water permeability.

The FT-IR was used to identify changes in chemical bonding in CNT/GO-PVA composite membranes. The FT-IR spectrum of CNT/GO-PVA composite membranes is shown in **Figure 2d.** The broad and stronger peaks for polar functional groups are visible for $CNT_{10}GO_{10}PVA_{0.5}$, $CNT_5GO_{15}PVA_{0.5}$ and, $GO_{20}PVA_{0.5}$ membranes, such as hydroxyl (-OH group) vibration peaks at 1435 cm^{-1} and 3000-3650 cm^{-1}. The broad peak could be attributed to hydrogen bonding between the polar functional groups of PVA and GO [37]. A less intense peak at 1650 cm^{-1} might be due to the carbonyl group of GO. However, all membranes lack another typical carbonyl peak at 1720 cm^{-1}, which could be due to the partial reduction of GO membranes. The peaks at 980 cm^{-1} and 1370 cm^{-1} are attributed to the stretching vibration of the C-O bond in CNT/GO-PVA composite membranes. Notably, the peaks are weaker than those on GO-based membranes, owing to the partial reduction of GO during membrane preparation [38]. Mild annealing of GO at 80 °C results in tailored nanosheet spacing while retaining the majority of the oxygen functionalities of GO. Thus, FTIR indicates that oxygen functional group linkages are weaker in $CNT_{15}GO_5PVA_{0.5}$ and $CNT_{10}GO_{10}PVA_{0.5}$ membranes than in $CNT_5GO_{15}PVA_{0.5}$ and $GO_{20}PVA_{0.5}$ membranes. Additionally, the acetyl ring exhibits peaks at 2845 and 1110 cm^{-1}, corresponding to the stretching vibrations of –CH and C–O–C bonds (**Figure 3b and c**) [39]. The deconvoluted FTIR spectra confirm the chemical bonding between GO and PVA for the $CNT_5GO_{15}PVA_{0.5}$ membrane (**Figure S4**). These peaks demonstrate the formation of a covalent bond between PVA and GO. The cross-linking and formation of covalent bonds between the PVA and GO moieties provide additional stability to the CNT/GO membrane, allowing it to overcome compaction and hydration effects.

The size of ordered domains, bonding nature, and the presence of dopants in the CNT/GO-PVA composite membranes was investigated using Raman spectroscopy [40]. **Figure 2e** shows the Raman spectra for CNT/GO-PVA composite membranes. Since membranes are prepared via pressure-assisted filtration technique, all membranes have a highly ordered structure. The D and G bands were prominent Raman peaks for all CNT/GO-PVA membranes. The G band peak at 1590 cm^{-1} is caused by the C-C bond stretching induced by the E_{2g} vibrational mode, whereas defects and disorders cause the D band peak at 1349 cm^{-1} in the graphite lattice induced by the A_{1g} vibrational mode. The relative intensity of the G band is greater for $CNT_{10}GO_{10}PVA_{0.5}$ and $CNT_{15}GO_5PVA_{0.5}$ membranes than for the other membranes, owing to the low amount of oxygen-containing functional groups. However, the relative intensity of the D band is greater in $CNT_5GO_{15}PVA_{0.5}$ and $GO_{20}PVA_{0.5}$ due to the presence of more polar functional groups that create defects at the micro-level. The values of I_D/I_G for $CNT_{15}GO_5PVA_{0.5}$, $CNT_{10}GO_{10}PVA_{0.5}$, $CNT_5GO_{15}PVA_{0.5}$, and $GO_{20}PVA_{0.5}$ are given 0.269, 0.273, 0.504, and 0.548, respectively. In contrast to standard sp^2 materials, reducing the defects in GO increases the I_D/I_G ratio. Hence, the $CNT_5GO_{15}PVA_{0.5}$ membrane showed a higher I_D/I_G ratio compared to $CNT_{15}GO_5PVA_{0.5}$ and $CNT_{10}GO_{10}PVA_{0.5}$ membranes. Notably, all CNT/GO-PVA composite membranes exhibited a transitional behaviour between ordered and disordered configurations. The $CNT_5GO_{15}PVA_{0.}$membranes had a Raman spectrum strikingly similar to that of the $GO_{20}PVA_{0.5}$ membrane. This indicates that the CNT is distributed throughout the matrix between the GO layers and around.

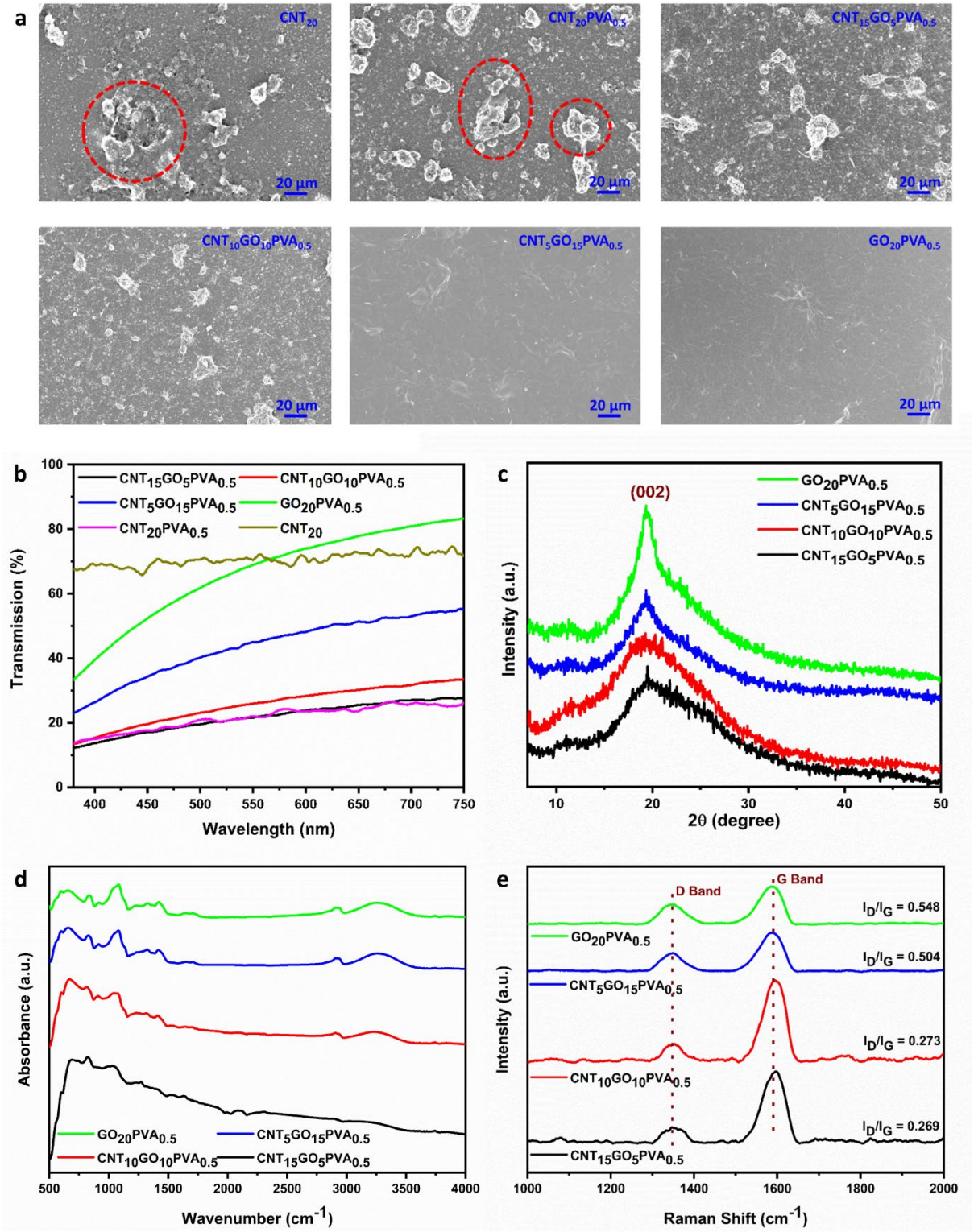

248

249 **Figure 2:** Physicochemical characterizations of CNT/GO-PVA composite membranes. (a) Top
250 surface morphology of CNT/GO-PVA composite membranes. (b) UV-visible spectra with
251 wavelength ranging from 380 to 750 nm. (c) XRD with 2θ ranging from 5 to 50 °. (d) FTIR

spectra with wavenumber ranging from 500 to 4000 cm^{-1}. (e) Raman spectra with Raman shift ranging from 1000-2000 cm^{-1}.

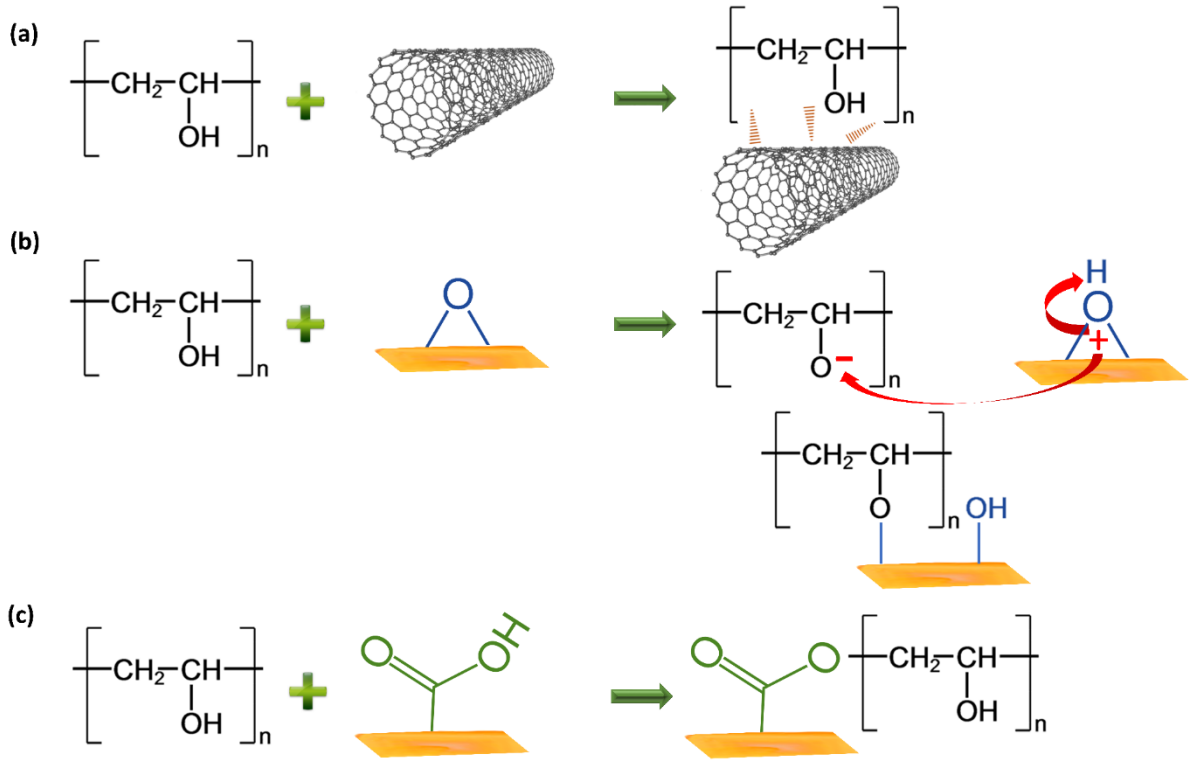

Figure 3: Schematic for the interaction scheme (a) Van der Waals interactions between PVA and CNT. (b) and (c) covalent bond formation between PVA and GO.

Water contact angle (WCA) studies were performed to determine the wettability of the CNT/GO-PVA composite membrane surfaces. The $CNT_5GO_{15}PVA_{0.5}$ and $GO_{20}PVA_{0.5}$ membranes showed lower WCA of 44.35 and 42.25, respectively. Hydroxyl, carboxyl, and other polar moieties on the membrane surface increase the membrane's hydrophilicity. By increasing the amount of CNT in the GO/PVA matrix, the WCA was increased to 48.95 and 56.42 of the $CNT_{10}GO_{10}PVA_{0.5}$ and the $CNT_{15}GO_5PVA_{0.5}$ membranes, respectively. Through Van der Waals force and π-π stacking interactions, non-polar CNT interacted with the GO/PVA matrix and thus occupied the space between the GO nanosheets and their external surface. The zeta potential (ζ) describes the charge on the surface of CNT/GO-PVA in their aqueous dispersions. It is an important physical parameter that can be used to investigate the effect of GO and PVA on the dispersion mechanism and quality of CNT/GO-PVA dispersions. **Table 2** shows the measurements of surface ζ measurements and water contact angle for CNT/GO-PVA composite membranes. For example, the surface ζ of $CNT_{15}GO_5PVA_{0.5}$ was

reduced to -11.9 mV. The surface ζ of the $CNT_5GO_{15}PVA_{0.5}$ and $GO_{20}PVA_{0.5}$ membranes was -26.1 and -30.3 mV, respectively, confirming the presence of polar functional groups on the membrane surface. However, pristine GO membranes show a surface ζ of up to -70 mV but suffer mechanical stability [18]. Therefore, PVA was used in this study to improve the stability of the CNT/GO membrane. The negative surface ζ of all the CNT/GO-PVA composite membranes is caused by deprotonation of carboxylic acid (–COOH) and hydroxyl groups (–OH) on the membrane surface derived from GO and PVA, respectively. As a result, resonance stabilization helps to stabilize the GO and PVA conjugate base [18]. Given this property, that resonance enables delocalization, the system's overall energy decreases as its electrons occupy a larger volume, thereby stabilizing the system. Whereas CNT can be classified into two distinct zones: i) end caps (hemispherical fullerene) and ii) sidewalls (folded graphene sheet). Usually, the GO polar functional groups interact with the end caps of CNT, and this process is driven by the release of strain energy [41, 42]. Also, the value of the acid dissociation constant fall in the range of 3.93-3.96 for GO; as a result, the ζ of CNT changes with the addition of GO solution [43]. The addition of CNT and PVA in between GO nanosheets reduces the availability of polar functional groups on the surface of the composite membranes. Thus, the surface ζ decreases with an increase in CNT concentration. Additionally, the surface ζ decreased due to the formation of covalent bonds between the GO and PVA moieties, as covalent bond formation consumes the extra electrons during the functionalization reaction (**Figure 3b** and **c**). The detailed interaction between CNT, PVA, and GO is shown in **Figure 3**.

Table 2: Surface zeta potential and water contact angle studies of CNT/GO-PVA composite membranes.

Membrane Code	Surface zeta potential (mV)	Water contact angle (°)
$CNT_5GO_{15}PVA_{0.5}$	-26.1 ± 0.8	44.35 ± 2.1
$CNT_{10}GO_{10}PVA_{0.5}$	-16.4 ± 1.3	48.95 ± 1.8
$CNT_{15}GO_5PVA_{0.5}$	-11.9 ± 0.7	56.42 ± 0.5
$GO_{20}PVA_{0.5}$	-30.3 ± 1.2	42.25 ± 1.4

XPS was used to analyse the surface chemistry and chemical state of CNT/GO-PVA composite membranes after mild annealing. **Figure 4** shows the deconvoluted C1s spectra of CNT/GO-PVA composite membranes, confirming the presence of CNT, GO, and PVA in the matrix. The C1s spectra are composed of several characteristics peaks with the typical peaks observed at 291 eV (O–C=O and π–π*), 289 eV (O–C=O), 288 eV (C=O), 287 eV (C–O), 286 eV (C–C/C=C), and 284 eV (C–O–C/C=O) confirms the presence of oxygen functionality in all membranes [44]. Since less GO was used in the $CNT_{15}GO_5PVA_{0.5}$ membrane, it contained a higher concentration of graphitic carbon, primarily C–C, as compared to others. The intensity of the sp^2 and sp^3 hybridized graphitic carbon (C-C) peak (286 eV) decreases in the following order $CNT_{15}GO_5PVA_{0.5} < CNT_{10}GO_{10}PVA_{0.5} < CNT_5GO_{15}PVA_{0.5} < GO_{20}PVA_{0.5}$. This could be because of the intercalation of CNT between consecutive GO nanosheets. Additionally, the $CNT_{15}GO_5PVA_{0.5}$ membrane had a lower intensity of the oxidised carbon peak due to the low concentration of GO in the matrix. Further, the peak for oxidized carbon at 287 eV (C–O) and 288 eV (C=O) of $CNT_5GO_{15}PVA_{0.5}$ membrane is identical to $GO_{20}PVA_{0.5}$ membrane.

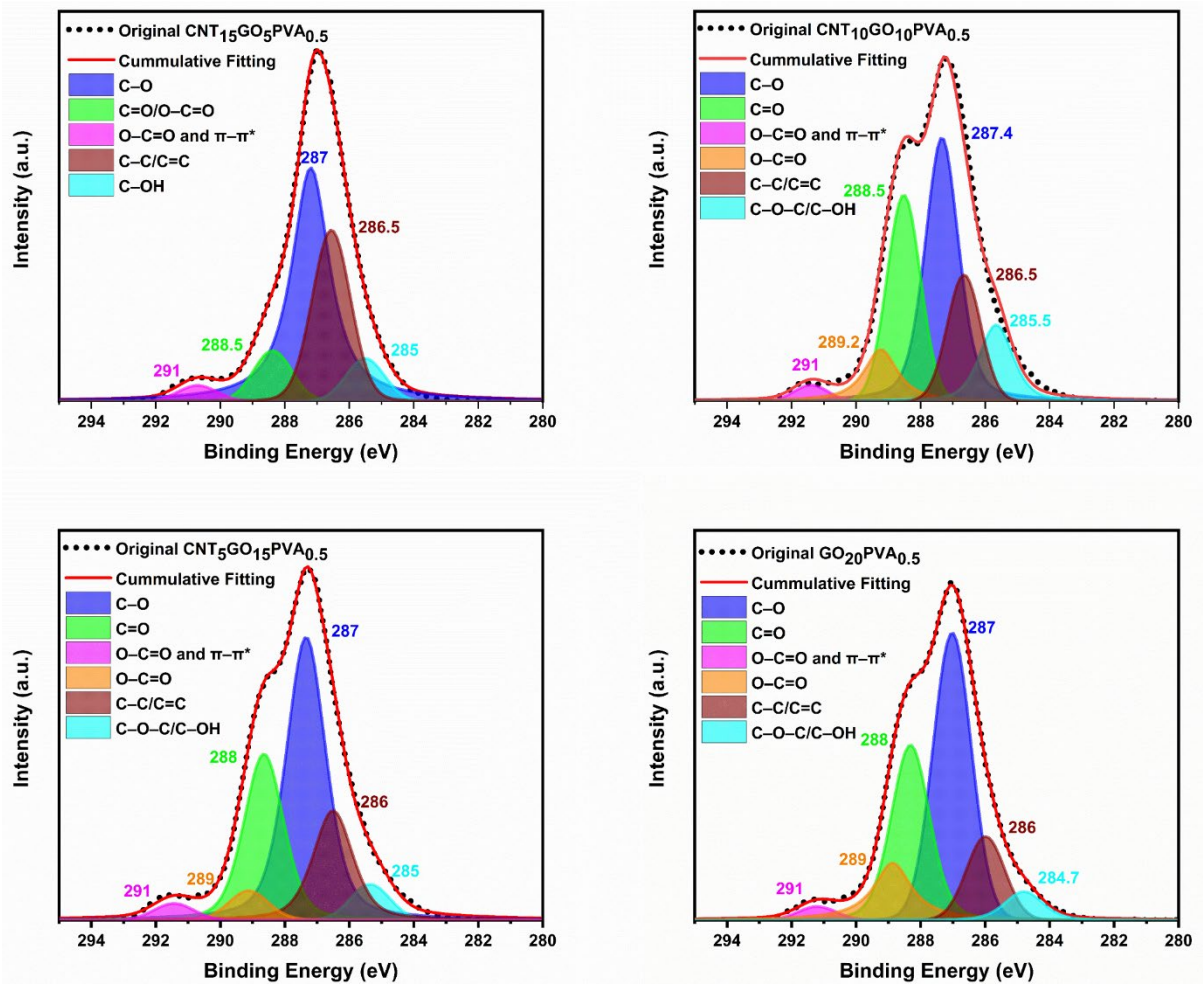

Figure 4: Deconvoluted C1s spectra of CNT/GO-PVA composite membranes.

3.2. Performance Studies

The permeability and selectivity of CNT/GO-PVA composite membranes for salt rejection were investigated using Na_2SO_4 and NaCl feed solutions at 2000 mg/L concentration. The permeation rate for Na_2SO_4 and NaCl solutions are shown in **Figures 5a** and **5b**, respectively. Water permeation rate for membranes is in the following order: $CNT_{15}GO_5PVA_{0.5}$ (8.9-8.15 LMH) < $CNT_{10}GO_{10}PVA_{0.5}$ (10.2-9.6 LMH) < $GO_{20}PVA_{0.5}$ (12.5-11.62 LMH) < $CNT_5GO_{15}PVA_{0.5}$ (14.2-13.45 LMH). The rapid water transport in all membranes is due to the combined effect of CNT, GO, and PVA. CNT's hydrophobic walls accelerate the flow of water molecules through the tube by causing them to "slip" whenever they come in contact with the walls [45, 46]. As the water molecules pass through the tube, they form a chain-like network with one another due to the presence of strong intramolecular hydrogen bonding [47, 48]. This improves the flow of water through the tubes and causes water molecules to be dragged forwards by the one ahead of them. Thus, a higher permeation rate is observed for the $CNT_5GO_{15}PVA_{0.5}$ membrane compared to the $GO_{20}PVA_{0.5}$ membrane. The combined effect of CNT and GO helps to get the desired permeation flux. In contrast, water transport in GO membranes occurs via the Grotthuss mechanism due to large oxygen-containing functional groups. Unlike CNT, water molecules follow a tortuous path between GO layers [10]. It is worth noting that a slight decrease in water flux was observed for all the membranes since the salt rejection experiments were performed using 2000 ppm of Na_2SO_4 and NaCl.

The rejection percentages for Na_2SO_4 and NaCl solutions are shown in **Figure 5c.** CNT/GO-PVA composite membranes rejects Na_2SO_4, and NaCl ions in the following decreasing order: $CNT_{15}GO_5PVA_{0.5}$ < $CNT_{10}GO_{10}PVA_{0.5}$ < $GO_{20}PVA_{0.5}$ < $CNT_5GO_{15}PVA_{0.5}$. The highest rejection rates of 94.2% and 85.86%, respectively, for Na_2SO_4 and NaCl, were achieved with the $CNT_5GO_{15}PVA_{0.5}$ membrane. In contrast, pristine $GO_{20}PVA_{0.5}$ membrane rejection rate was 92.1% for Na_2SO_4 and 83.5% for NaCl ions. The desalination performance of CNT/GO-PVA composite membranes (**Figure 5d**) is mainly attributed to i) size-exclusion mechanism, ii) electrostatic interactions between negatively charged CNT/GO-PVA composite membranes and feed salt solutions, and iii) ion adsorption on the surface of CNT/GO-PVA composite membranes.

In this study, Na_2SO_4 has a higher rejection rate than NaCl for two primary reasons that may seem counterintuitive. Firstly, Na_2SO_4 has a higher molecular weight, and the sulphate ion (SO_4^{-2}; 0.258 nm) has a larger ionic radius than the chloride (Cl^{-1}; 0.175 nm) ion. Thus, technically, it is more difficult for the SO_4^{-2} to pass through the membrane. Second, the membranes are negatively charged, as shown in surface zeta potential measurements, and the SO_4^{-2} has a greater negative charge than the Cl^{-1}. Thus, long-range interactions such as electrostatic repulsions between the negatively charged SO_4^{-2} and the negatively charged membrane surface are higher than those with Cl^{-1} ion. Similar results were reported by Hung et al. for GO-graphene membranes [18]. The addition of graphene improved the water permeability of the GO membrane and salt rejection in the following order NaCl < magnesium chloride ($MgCl_2$) < magnesium sulphate ($MgSO_4$) < Na_2SO_4.

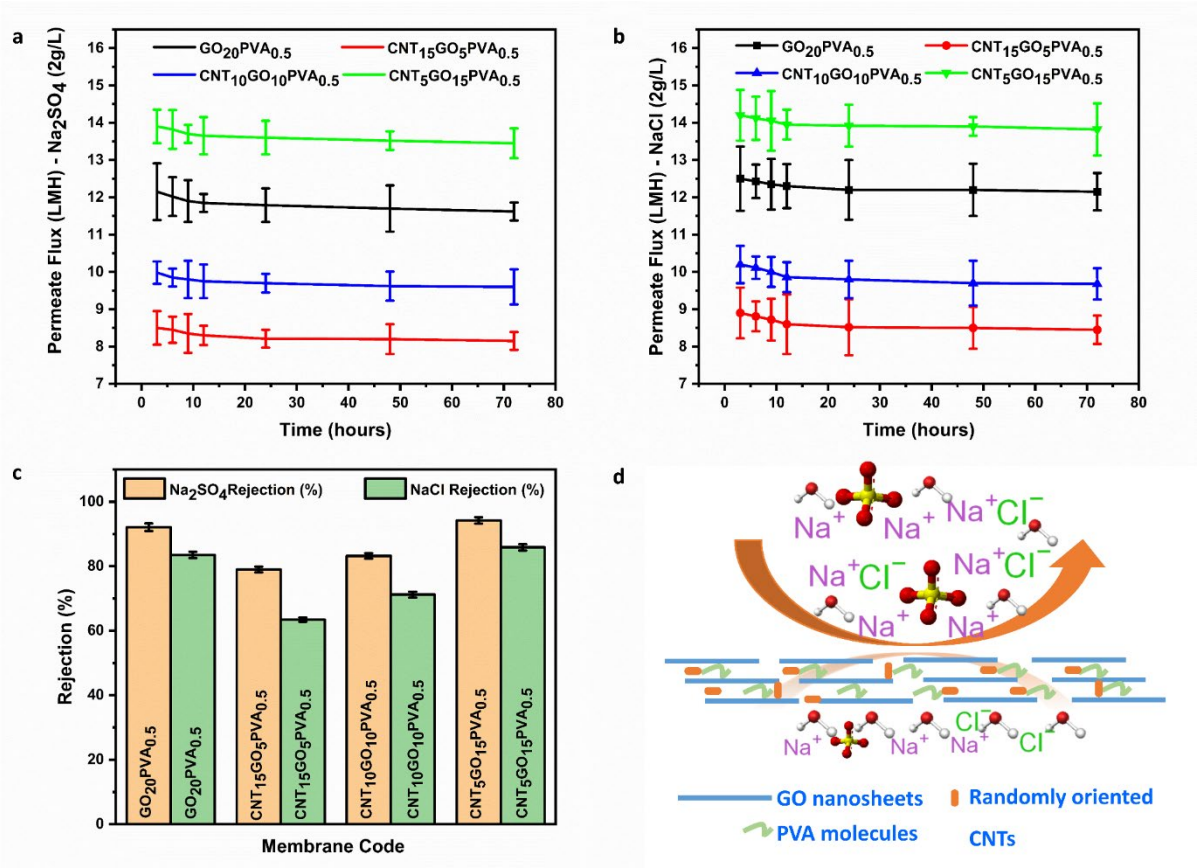

Figure 5: Na_2SO_4 (a), and NaCl (b) flux of CNT/GO-PVA composite membranes. (c) The rejection rate of Na_2SO_4 and NaCl for CNT/GO-PVA composite membranes. (d) Illustration for the desalination performance of CNT/GO-PVA composite membranes.

Table 3 shows the comparison between CNT/GO-PVA composite membranes and previously reported GO-based membranes. Parsamehr and colleagues cross-linked GO with polyethyleneimine (PEI) to improve the membrane's stability and achieved a rejection rate of 37.5% for NaCl [49]. Similarly, tannic acid (TA), 1-Ethyl-3-(3-dimethylaminopropyl) carbodiimide (EDC), and N-Hydroxysuccinimide (NHS) are added to GO to improve separation performance [49, 50]. We previously investigated the effect of molybdenum disulphide as a nanospacer and PVA as a cross-linker on NaCl rejection and achieved up to 89 % rejection [11]. Additionally, the low permeability of 4.19 LMH for GO/MoS_2-PVA membranes precludes application at a larger scale [11]. Recently, Li et al. investigated the effect of annealing on GO membranes and concluded that mild annealing enables more ordered laminar channels in GO membranes. Additionally, the authors reported a high permeability of 29.48 LMH and a moderate rejection for Na_2SO_4 of 57.73% [51]. In another study, researchers used single-walled CNT (SWCNT) between GO nanosheets achieved a 97.5% rejection rate of an organic dye. However, the operation time and membrane stability remained an issue [30]. Although numerous simulation studies confirmed carbon nanotubes' superior desalination performance, experimental validation is still pending [46, 52]. In the present study, optimized CNT is used as a nanospacer to increase permeability up to 14.2 LMH, with a high rejection rate of 94.2% and 85.86% of Na_2SO_4 and NaCl, respectively. **Table 3** shows that $CNT_5GO_{15}PVA_{0.5}$ membrane in this study achieved the highest rejection rate and moderate permeation flow rate.

Overall, the CNT/GO-PVA membranes showed over 85.86% rejection of NaCl, the ionic radii of Na^+ (0.102 nm) and Cl^- (0.175 nm). The membranes are also expected to have higher rejection for ions of larger ionic radii, such as sulfate. In other words, the membranes will exhibit higher rejection to divalent or large molecular weight ions that the membrane can reject by size exclusion or electrostatic repulsion. Notably, a lower rejection rate was observed for NaCl than Na_2SO_4 due to the higher ionic radii of sulfate anion (SO_4^{2-}) compared to chloride ion (Cl^-). Additionally, the SO_4^{2-} anion exhibits greater electrostatic repulsion with CNT/GO-PVA composite membranes than the Cl^- anion does due to the additional negative charge. Therefore, the selectivity of CNT/GO-PVA composite membranes is due to the combined effect of molecular size and charge density.

Table 3: Comparison of CNT/GO-PVA composite membrane performance with others reported in the literature.

Membrane code	Substrate	Permeability (LMH)	Rejection	Reference
Pristine GO	CA	10	37.5% NaCl	[49]
Activated GO-PEI	CA	7	55% NaCl	[49]
GO/MoS_2-PVA	CA	4.19	89.93% NaCl	[11]
TA-GO-PEI	CA	15	64% NaCl	[50]
GO-PEI (layer-by-layer)	PP	4.2	38% NaCl	[53]
Base-Refluxing Reduced GO	MCE	22.82	40% NaCl	[54]
Mild annealed GO	PES	29.48	57.73% Na_2SO_4	[51]
Hybrid rGO-CNT	AA0	20-30	97.13% MO	[32]
FCNT-GONR	polymeric support	138	100% organic dyes	[55]
Hybrid rGO-GONR	Nylon support	161-327	95.13% MO >99% MR	[56]
$CNT_5GO_{15}PVA_{0.5}$	MCE	13.45-14.2	94.2% Na_2SO_4 85.86% NaCl	Present work
$GO_{20}PVA_{0.5}$	MCE	11.62-12.5	92.1% Na_2SO_4 83.5% NaCl	Present work

GO: graphene oxide; PEI: polyethyleneimine; MoS_2: molybdenum disulfide; PVA: polyvinyl alcohol; TA: tannic acid; CNT: carbon nanotube; CA: cellulose acetate; PP: polypropylene; MCE mixed cellulose esters; AAO: anodic aluminium oxide; GONR: graphene oxide nanoribbon; FCNT: functionalized carbon nanotube; PES: polyethersulfone; NaCl: sodium chloride; Na_2SO_4: sodium sulphate; MR: methyl orange and MO: methyl orange

4. Conclusion

In conclusion, the pressure-assisted filtration technique successfully prepared stable covalent cross-linked CNT/GO-PVA composite membranes. The prepared membranes had excellent performance for the salt rejection with permeation rate at low operating pressure. Covalent cross-linkage between GO and PVA prevents the GO nanosheets from swelling and

disintegration. In contrast, mild annealing and CNT improved the CNT/GO-PVA membranes water permeability. FTIR, Raman, XRD, XPS, and surface zeta potential analysis discussed chemical bonding and structural properties. CNT/GO-PVA composite membranes are highly stable under dead-end filtration tests for 72 hours with enhanced permeability and selectivity. $CNT_5GO_{15}PVA_{0.5}$ membrane achieved over 94% rejection rate to Na_2SO_4 and 13.45 LMH water flux, and for the NaCl, the rejection rate was 85.86%, and water flux was 14.2 LMH. The combination of 1D-CNT and 2D-GO nanosheets proved to be an attractive strategy to prepare next-generation membranes.

References

[1] D.L. Oatley-Radcliffe, M. Walters, T.J. Ainscough, P.M. Williams, A.W. Mohammad, N. Hilal, Nanofiltration membranes and processes: A review of research trends over the past decade, Journal of Water Process Engineering, 19 (2017) 164-171.

[2] J. Kang, Y. Choi, J.H. Kim, E. Choi, S.E. Choi, O. Kwon, D.W. Kim, Functionalized nanoporous graphene membrane with ultrafast and stable nanofiltration, J. Membr. Sci., 618 (2021) 118635.

[3] P. Bhol, S. Yadav, A. Altaee, M. Saxena, P.K. Misra, A.K. Samal, Graphene-Based Membranes for Water and Wastewater Treatment: A Review, ACS Applied Nano Materials, 4 (2021) 3274-3293.

[4] N.L. Le, S.P. Nunes, Materials and membrane technologies for water and energy sustainability, Sustainable Materials and Technologies, 7 (2016) 1-28.

[5] R. Kingsbury, J. Wang, O. Coronell, Comparison of water and salt transport properties of ion exchange, reverse osmosis, and nanofiltration membranes for desalination and energy applications, J. Membr. Sci., (2020) 117998.

[6] S. Huang, M.-B. Wu, C.-Y. Zhu, M.-Q. Ma, J. Yang, J. Wu, Z.-K. Xu, Polyamide nanofiltration membranes incorporated with cellulose nanocrystals for enhanced water flux and chlorine resistance, ACS Sustainable Chemistry & Engineering, 7 (2019) 12315-12322.

[7] A. Anand, B. Unnikrishnan, J.-Y. Mao, H.-J. Lin, C.-C. Huang, Graphene-based nanofiltration membranes for improving salt rejection, water flux and antifouling–A review, Desalination, 429 (2018) 119-133.

[8] S. Yadav, H. Saleem, I. Ibrar, O. Naji, A.A. Hawari, A.A. Alanezi, S.J. Zaidi, A. Altaee, J. Zhou, Recent developments in forward osmosis membranes using carbon-based nanomaterials, Desalination, 482 (2020) 114375.

[9] C.A. Ruiz-Torres, J. Kang, K.M. Kang, K.M. Cho, Y.T. Nam, C. Byon, Y.-Y. Chang, D.W. Kim, H.-T. Jung, Graphene-based ultrafast nanofiltration membrane under cross-flow operation: Effect of high-flux and filtered solute on membrane performance, Carbon, 185 (2021) 641-649.

[10] R. Joshi, P. Carbone, F.-C. Wang, V.G. Kravets, Y. Su, I.V. Grigorieva, H. Wu, A.K. Geim, R.R. Nair, Precise and ultrafast molecular sieving through graphene oxide membranes, Science, 343 (2014) 752-754.

[11] S. Yadav, I. Ibrar, A. Altaee, A.K. Samal, R. Ghobadi, J. Zhou, Feasibility of brackish water and landfill leachate treatment by GO/MoS2-PVA composite membranes, Sci. Total Environ., (2020) 141088.

[12] C. Wang, M.J. Park, D.H. Seo, H.K. Shon, Inkjet Printing of Graphene Oxide and Dopamine on Nanofiltration Membranes for Improved Anti-fouling Properties and Chlorine Resistance, Sep. Purif. Technol., (2020) 117604.

[13] R. Zeynali, K. Ghasemzadeh, A.B. Sarand, F. Kheiri, A. Basile, Performance evaluation of graphene oxide (GO) nanocomposite membrane for hydrogen separation: Effect of dip coating sol concentration, Sep. Purif. Technol., 200 (2018) 169-176.

[14] C.-H. Tsou, Q.-F. An, S.-C. Lo, M. De Guzman, W.-S. Hung, C.-C. Hu, K.-R. Lee, J.-Y. Lai, Effect of microstructure of graphene oxide fabricated through different self-assembly techniques on 1-butanol dehydration, J. Membr. Sci., 477 (2015) 93-100.

[15] S. Zheng, Q. Tu, J.J. Urban, S. Li, B. Mi, Swelling of graphene oxide membranes in aqueous solution: characterization of interlayer spacing and insight into water transport mechanisms, ACS nano, 11 (2017) 6440-6450.

[16] M. Zhang, K. Guan, Y. Ji, G. Liu, W. Jin, N. Xu, Controllable ion transport by surface-charged graphene oxide membrane, Nature communications, 10 (2019) 1-8.

[17] Y. Wei, Y. Zhang, X. Gao, Z. Ma, X. Wang, C. Gao, Multilayered graphene oxide membranes for water treatment: A review, Carbon, 139 (2018) 964-981.

[18] W.-S. Hung, T.-J. Lin, Y.-H. Chiao, A. Sengupta, Y.-C. Hsiao, S.R. Wickramasinghe, C.-C. Hu, K.-R. Lee, J.-Y. Lai, Graphene-induced tuning of the d-spacing of graphene oxide composite nanofiltration

membranes for frictionless capillary action-induced enhancement of water permeability, Journal of Materials Chemistry A, 6 (2018) 19445-19454.
[19] W.-S. Hung, C.-H. Tsou, M. De Guzman, Q.-F. An, Y.-L. Liu, Y.-M. Zhang, C.-C. Hu, K.-R. Lee, J.-Y. Lai, Cross-linking with diamine monomers to prepare composite graphene oxide-framework membranes with varying d-spacing, Chemistry of Materials, 26 (2014) 2983-2990.
[20] L. Huang, J. Chen, T. Gao, M. Zhang, Y. Li, L. Dai, L. Qu, G. Shi, Reduced graphene oxide membranes for ultrafast organic solvent nanofiltration, Adv. Mater., 28 (2016) 8669-8674.
[21] H.-H. Huang, R.K. Joshi, K.K.H. De Silva, R. Badam, M. Yoshimura, Fabrication of reduced graphene oxide membranes for water desalination, J. Membr. Sci., 572 (2019) 12-19.
[22] J.R. Werber, C.O. Osuji, M. Elimelech, Materials for next-generation desalination and water purification membranes, Nature Reviews Materials, 1 (2016) 1-15.
[23] W. Choi, K.-Y. Chun, J. Kim, C.-S. Han, Ion transport through thermally reduced and mechanically stretched graphene oxide membrane, Carbon, 114 (2017) 377-382.
[24] K.S. Andrikopoulos, G. Bounos, D. Tasis, L. Sygellou, V. Drakopoulos, G.A. Voyiatzis, The effect of thermal reduction on the water vapor permeation in graphene oxide membranes, Advanced Materials Interfaces, 1 (2014) 1400250.
[25] C.P. Athanasekou, S. Morales-Torres, V. Likodimos, G.E. Romanos, L.M. Pastrana-Martinez, P. Falaras, D.D. Dionysiou, J.L. Faria, J.L. Figueiredo, A.M. Silva, Prototype composite membranes of partially reduced graphene oxide/TiO2 for photocatalytic ultrafiltration water treatment under visible light, Applied Catalysis B: Environmental, 158 (2014) 361-372.
[26] W. Wang, E. Eftekhari, G. Zhu, X. Zhang, Z. Yan, Q. Li, Graphene oxide membranes with tunable permeability due to embedded carbon dots, Chem. Commun., 50 (2014) 13089-13092.
[27] A. Nicolaï, B.G. Sumpter, V. Meunier, Tunable water desalination across graphene oxide framework membranes, Physical Chemistry Chemical Physics, 16 (2014) 8646-8654.
[28] M. Hu, B. Mi, Enabling graphene oxide nanosheets as water separation membranes, Environ. Sci. Technol., 47 (2013) 3715-3723.
[29] Y. Han, Y. Jiang, C. Gao, High-flux graphene oxide nanofiltration membrane intercalated by carbon nanotubes, ACS applied materials & interfaces, 7 (2015) 8147-8155.
[30] S.J. Gao, H. Qin, P. Liu, J. Jin, SWCNT-intercalated GO ultrathin films for ultrafast separation of molecules, Journal of Materials Chemistry A, 3 (2015) 6649-6654.
[31] J. Zou, L. Liu, H. Chen, S.I. Khondaker, R.D. McCullough, Q. Huo, L. Zhai, Dispersion of pristine carbon nanotubes using conjugated block copolymers, Adv. Mater., 20 (2008) 2055-2060.
[32] X. Chen, M. Qiu, H. Ding, K. Fu, Y. Fan, A reduced graphene oxide nanofiltration membrane intercalated by well-dispersed carbon nanotubes for drinking water purification, Nanoscale, 8 (2016) 5696-5705.
[33] Y. Wang, Y. Liu, Y. Yu, H. Huang, Influence of CNT-rGO composite structures on their permeability and selectivity for membrane water treatment, Journal of Membrane Science, 551 (2018) 326-332.
[34] Y. Wu, C.-F. Fu, Q. Huang, P. Zhang, P. Cui, J. Ran, J. Yang, T. Xu, 2D Heterostructured Nanofluidic Channels for Enhanced Desalination Performance of Graphene Oxide Membranes, ACS nano, 15 (2021) 7586-7595.
[35] G. Yang, Z. Xie, M. Cran, D. Ng, S. Gray, Enhanced desalination performance of poly (vinyl alcohol)/carbon nanotube composite pervaporation membranes via interfacial engineering, J. Membr. Sci., 579 (2019) 40-51.
[36] W.L. Xu, C. Fang, F. Zhou, Z. Song, Q. Liu, R. Qiao, M. Yu, Self-assembly: a facile way of forming ultrathin, high-performance graphene oxide membranes for water purification, Nano letters, 17 (2017) 2928-2933.
[37] S. Morimune, T. Nishino, T. Goto, Poly (vinyl alcohol)/graphene oxide nanocomposites prepared by a simple eco-process, Polym. J., 44 (2012) 1056-1063.
[38] Y. Zhang, T.-S. Chung, Graphene oxide membranes for nanofiltration, Current opinion in chemical engineering, 16 (2017) 9-15.

503 [39] C. Cheng, L. Shen, X. Yu, Y. Yang, X. Li, X. Wang, Robust construction of a graphene oxide barrier
504 layer on a nanofibrous substrate assisted by the flexible poly (vinylalcohol) for efficient pervaporation
505 desalination, Journal of Materials Chemistry A, 5 (2017) 3558-3568.
506 [40] J. Chen, X. Shi, L. Ren, Y. Wang, Graphene oxide/PVA inorganic/organic interpenetrating hydrogels
507 with excellent mechanical properties and biocompatibility, Carbon, 111 (2017) 18-27.
508 [41] F.H. Gojny, J. Nastalczyk, Z. Roslaniec, K. Schulte, Surface modified multi-walled carbon nanotubes
509 in CNT/epoxy-composites, Chem. Phys. Lett., 370 (2003) 820-824.
510 [42] N. Karousis, N. Tagmatarchis, D. Tasis, Current progress on the chemical modification of carbon
511 nanotubes, Chemical reviews, 110 (2010) 5366-5397.
512 [43] A.M. Dimiev, L.B. Alemany, J.M. Tour, Graphene oxide. Origin of acidity, its instability in water,
513 and a new dynamic structural model, ACS nano, 7 (2013) 576-588.
514 [44] Y.-R. Son, S.-J. Park, Green preparation and characterization of graphene oxide/carbon
515 nanotubes-loaded carboxymethyl cellulose nanocomposites, Sci. Rep., 8 (2018) 1-10.
516 [45] S.K. Kannam, P.J. Daivis, B. Todd, Modeling slip and flow enhancement of water in carbon
517 nanotubes, MRS Bull., 42 (2017) 283-288.
518 [46] S. Joseph, N. Aluru, Why are carbon nanotubes fast transporters of water?, Nano Lett., 8 (2008)
519 452-458.
520 [47] M. Majumder, N. Chopra, R. Andrews, B.J. Hinds, Enhanced flow in carbon nanotubes, Nature,
521 438 (2005) 44-44.
522 [48] J.A. Thomas, A.J. McGaughey, Reassessing fast water transport through carbon nanotubes, Nano
523 Lett., 8 (2008) 2788-2793.
524 [49] P.S. Parsamehr, M. Zahed, M.A. Tofighy, T. Mohammadi, M. Rezakazemi, Preparation of novel
525 cross-linked graphene oxide membrane for desalination applications using (EDC and NHS)-activated
526 graphene oxide and PEI, Desalination, 468 (2019) 114079.
527 [50] M.-Y. Lim, Y.-S. Choi, J. Kim, K. Kim, H. Shin, J.-J. Kim, D.M. Shin, J.-C. Lee, Cross-linked graphene
528 oxide membrane having high ion selectivity and antibacterial activity prepared using tannic acid-
529 functionalized graphene oxide and polyethyleneimine, Journal of Membrane Science, 521 (2017) 1-9.
530 [51] Y. Li, S. Yuan, Y. Xia, W. Zhao, C.D. Easton, C. Selomulya, X. Zhang, Mild annealing reduced
531 graphene oxide membrane for nanofiltration, J. Membr. Sci., 601 (2020) 117900.
532 [52] A.O. Rashed, A. Merenda, T. Kondo, M. Lima, J. Razal, L. Kong, C. Huynh, L.F. Dumée, Carbon
533 nanotube membranes-strategies and challenges towards scalable manufacturing and practical
534 separation applications, Separation and Purification Technology, (2020) 117929.
535 [53] Z. Jia, Y. Wang, Covalently crosslinked graphene oxide membranes by esterification reactions for
536 ions separation, Journal of Materials Chemistry A, 3 (2015) 4405-4412.
537 [54] Y. Han, Z. Xu, C. Gao, Ultrathin graphene nanofiltration membrane for water purification,
538 Advanced Functional Materials, 23 (2013) 3693-3700.
539 [55] Y. Choi, J. Kang, E. Choi, J.Y. Kim, J.P. Kim, J.H. Kim, O. Kwon, D.W. Kim, Carbon nanotube-
540 supported graphene oxide nanoribbon bilayer membrane for high-performance diafiltration,
541 Chemical Engineering Journal, 427 (2022) 131805.
542 [56] K.M. Cho, H.-J. Lee, Y.T. Nam, Y.-J. Kim, C. Kim, K.M. Kang, C.A. Ruiz Torres, D.W. Kim, H.-T. Jung,
543 Ultrafast-selective nanofiltration of an hybrid membrane comprising laminated reduced graphene
544 oxide/graphene oxide nanoribbons, ACS applied materials & interfaces, 11 (2019) 27004-27010.

545

546

547

548

Supplementary Information

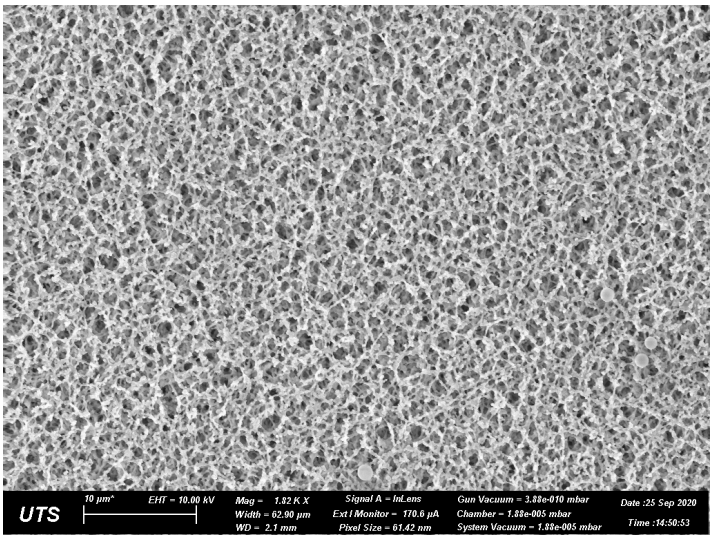

Figure S1: FESEM image for hydrophilic mixed cellulose esters (MCE) substrate.

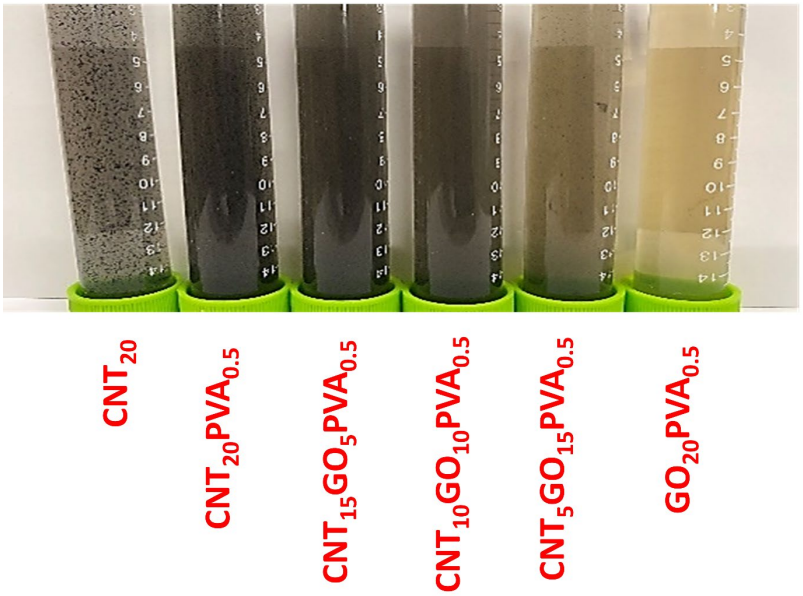

560

561 **Figure S2:** Aqueous suspensions of CNT/GO-PVA used for the membrane fabrication.

562

563

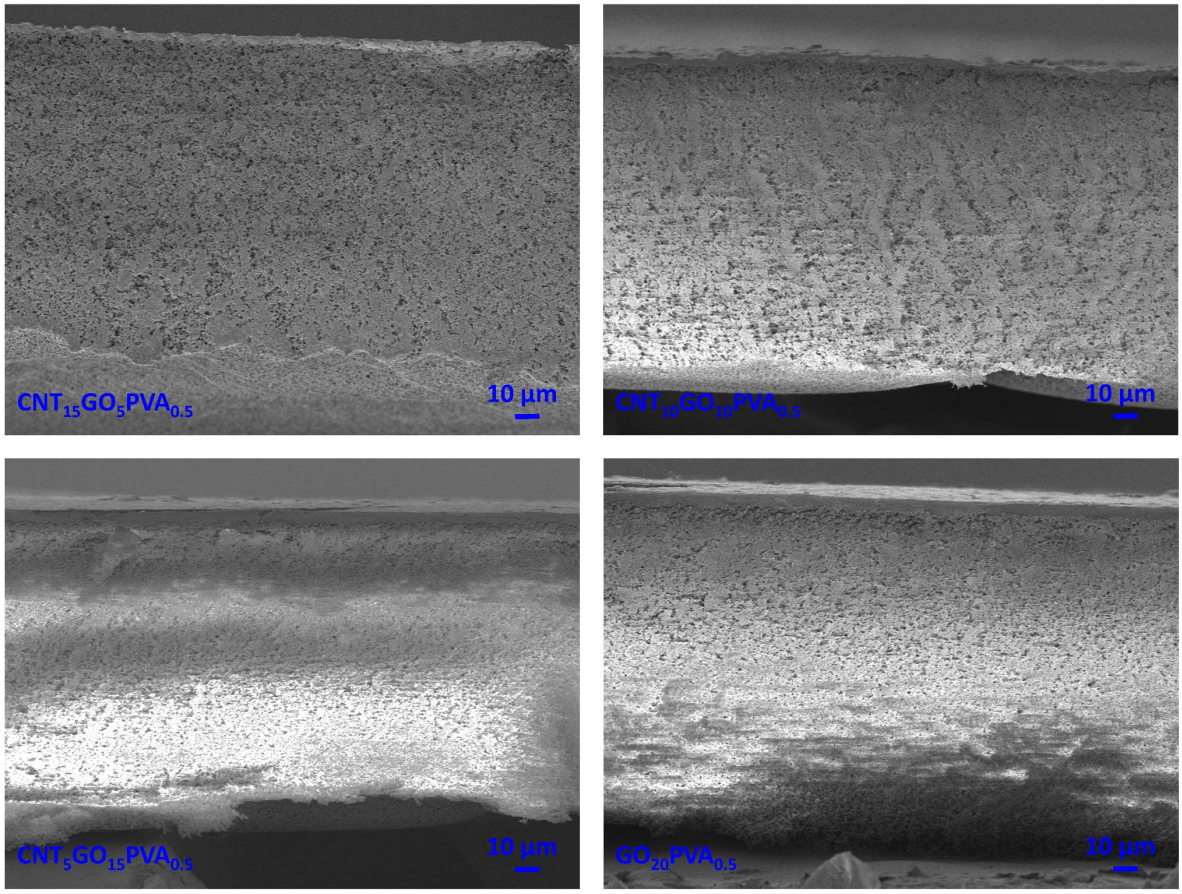

564

565 **Figure S3:** Cross-sectional morphology of CNT/GO-PVA composite membranes.

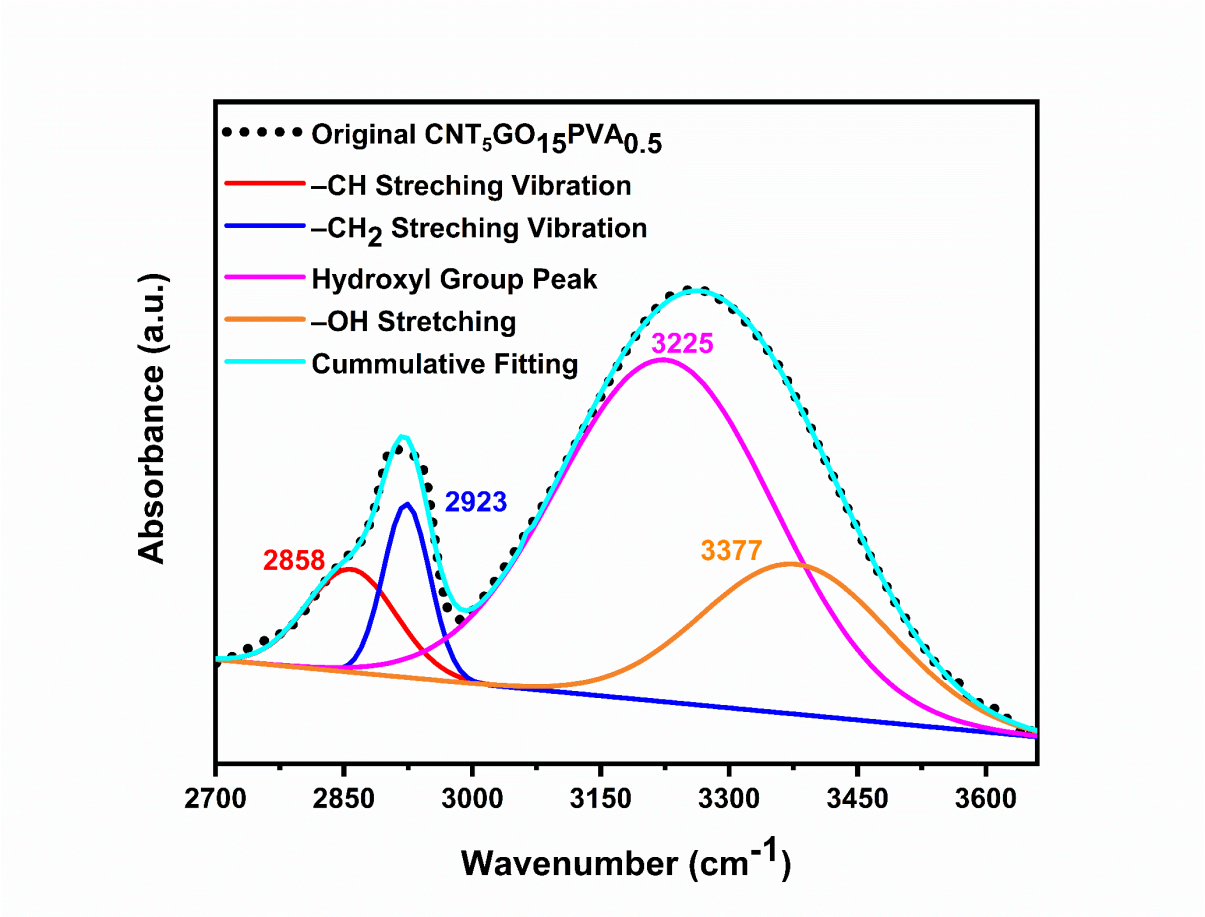

566
567 **Figure S4:** Deconvoluted FTIR spectra of $CNT_5GO_{15}PVA_{0.5}$ membrane.

568

569